Appendix C. Coulomb Fracture Criterion

Our results for the chapters of this thesis use the Hencky-Mises plastic yield criterion because of its simplicity. We demonstrate with this criterion a bias toward the stress rate, $\dot{\boldsymbol{\sigma}}_T$, for medium to large heterogeneity ratios, HR, which is a measure of the magnitude of the spatially heterogeneous stress relative to the spatial mean stress, $\dot{\boldsymbol{\sigma}}_B$. One question that arises is, do we still see this bias if we use the more common Coulomb Failure criterion. The answer is yes, but the P-T plots become more complicated because the two conjugate planes are not perpendicular. Each conjugate plane now has its own set of P-T axes.

Figure C.1 shows a Mohr circle diagram to visualize our Coulomb Failure. Note, elsewhere in this thesis, we have used the physics convention that tensile principal stresses are > 0, and compressive principal stresses are < 0. For this appendix, however, we will use the opposite convention: tensile principal stresses are < 0, and compressive principal stresses are > 0, which is the common convention when working with Mohr's circles. Therefore in Figure C.1, σ_1 is our most compressive principal stress, and σ_3 is the least compressive principal stress. τ is the shear stress axis, σ_n is the normal stress axis, and the line elevated at angle ϕ represents the failure threshold for Coulomb Failure. The value, τ_0, represents any cohesion in the material. In our simulations, we want to generate fresh fractures; therefore, for Coulomb Failure, we solve for where the circle (representing the outer set of shear stress/normal stress values) is tangent to the failure threshold. Last, the angle θ represents the angle between the failure plane and the most compressive principal stress, σ_1.

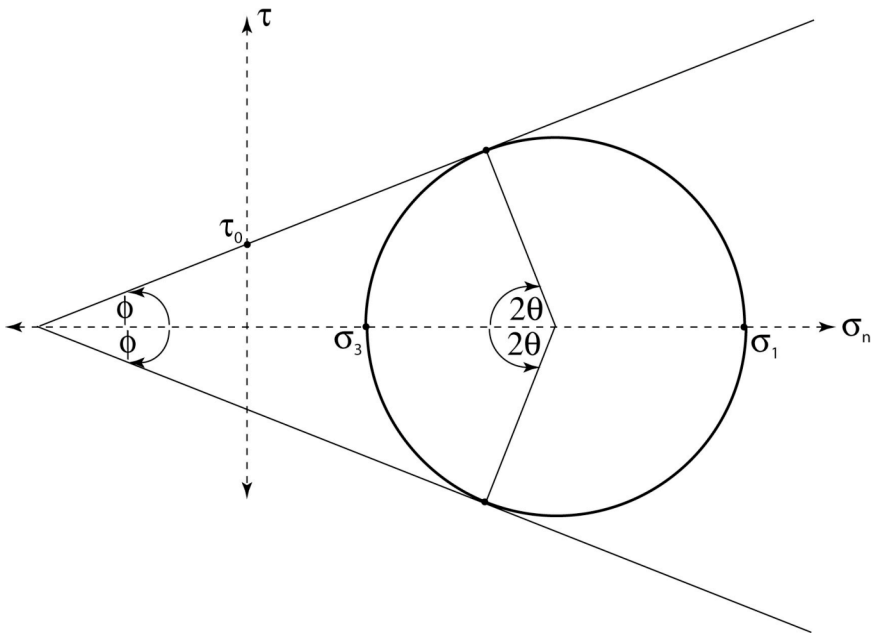

Figure C.1. *Mohr circle and Coulomb Failure Criterion. On the axes of shear stress,* τ*, vs. normal stress,* σ_n*, the principal stresses,* σ_1 *(most compressive principal stress) and* σ_3 *(least compressive principal stress), define the Mohr's circle. The outside circumference of the Mohr's circle shown specifies the set of* τ*,* σ_n *values for all orientations of planes whose normals lie in the plane of* σ_1 *and* σ_3*. The line elevated at an angle,* ϕ*, specifies the failure threshold for the Coulomb Failure Criterion, where* $\mu = \tan\phi$*, and* τ_0 *is the cohesion of the material. Failure thus occurs where the line is tangent to the plane. In our simulations of Coulomb Failure, we solve for the time,* t*, when the Mohr circle becomes tangent to the failure line. Once failure occurs,* θ *describes the angle between the failure planes and* σ_1*. For* $\mu = 0.0$*,* $\theta = 45°$ *and the conjugate failure planes are perpendicular. This is the same as the maximally oriented planes we calculate in our plastic yield criterion. For* $\mu > 0.0$ *we find* $\theta < 45°$*. In addition, the conjugate failure planes are no longer perpendicular, resulting in two sets of P-T axes per failure (Figure C.3).*

The coefficient of friction, μ, is defined as

$$\mu = \tan\phi; \tag{C.1}$$

therefore, the failure threshold can be described with the following equation,

$$\tau = \tau_0 + \mu\sigma_n. \tag{C.2}$$

The Mohr circle can be described with,

$$\left(\sigma_n - \sigma_C\right)^2 + \tau^2 = r^2 \tag{C.3}$$

where the center point is

$$\sigma_C = \frac{\sigma_1 + \sigma_3}{2} \tag{C.4}$$

and the radius is

$$r = \frac{\sigma_1 - \sigma_3}{2}. \tag{C.5}$$

Substituting Equations (C.4) and (C.5) into Equation (C.3) we have the following description of the Mohr circles:

$$\left(\sigma_n - \frac{\sigma_1 + \sigma_3}{2}\right)^2 + \tau^2 = \left(\frac{\sigma_1 - \sigma_3}{2}\right)^2. \tag{C.6}$$

If we solve for τ we have,

$$\tau = \pm\sqrt{\sigma_n\left(\sigma_1 + \sigma_3\right) - \sigma_n^2 - \sigma_1\sigma_3} \tag{C.7}$$

where the positive solution represents the top half of the Mohr circle and the negative solution represents the bottom half of the Mohr circle.

The two failure planes are $\pm\theta$ relative to the σ_1 axes, so if we solve for one failure plane we know the other. Let us set the positive solution of Equation (C.7) equal

to $\tau = \tau_0 + \mu\sigma_n$ so that the Mohr circle is tangent to the failure line, and then solve for the normal stress, σ_n, at this failure point,

$$\sigma_n = \frac{\left(\sigma_1 + \sigma_3 - 2\tau_0\mu\right) \pm \sqrt{\left(\sigma_1 + \sigma_3 - 2\tau_0\mu\right)^2 - 4\left(\mu^2 + 1\right)\left(\tau_0^2 + \sigma_1\sigma_3\right)}}{2\left(\mu^2 + 1\right)}. \qquad \text{(C.8)}$$

We want solutions where $\tau^+ = \tau^-$ or $\sigma_n^+ = \sigma_n^-$; therefore, we want the $+$ and $-$ solutions to Equation (C.8) to equal one another. This means that the second quantity in the numerator should equal zero,

$$\sqrt{\left(\sigma_1 + \sigma_3 - 2\tau_0\mu\right)^2 - 4\left(\mu^2 + 1\right)\left(\tau_0^2 + \sigma_1\sigma_3\right)} = 0. \qquad \text{(C.9)}$$

Solving for σ_1 in terms of σ_3,

$$\sigma_1 = \left(1 + 2\mu^2\right)\sigma_3 + 2\tau_0\mu \pm 2\sqrt{\left(1 + \mu^2\right)}\left(\mu\sigma_3 + \tau_0\right). \qquad \text{(C.10)}$$

We want σ_1 to increase when σ_3 increases; thus, we choose the positive root to give the final equation for the relation between σ_1 and σ_3,

$$\sigma_1 = \left[1 + 2\mu^2 + 2\mu\sqrt{\left(1 + \mu^2\right)}\right]\sigma_3 + 2\left[\mu + \sqrt{\left(1 + \mu^2\right)}\right]\tau_0. \qquad \text{(C.11)}$$

One of our first questions about this equation is, over what range of values is it valid. We find that it is valid for $\sigma_3 > -\frac{\tau_0}{\mu}$; specifically, the least compressive principal stress, σ_3, must be greater than the intercept with the σ_n axis at $\tau = 0.0$.

Of interest, when we solve Equation (C.11) in terms of the cohesion, τ_0,

$$\tau_0 = \frac{\sigma_1 - \left[1 + 2\mu^2 + 2\mu\sqrt{\left(1 + \mu^2\right)}\right]\sigma_3}{2\left[\mu + \sqrt{\left(1 + \mu^2\right)}\right]} \qquad \text{(C.12)}$$

and set the coefficient of friction to zero, $\mu = 0.0$, we find that

$$\tau_0 = \frac{\sigma_1 - \sigma_3}{2} \qquad \text{for } \mu = 0.0, \tag{C.13}$$

and that Equation (C.2) becomes

$$\tau = \frac{\sigma_1 - \sigma_3}{2} \qquad \text{for } \mu = 0.0, \tag{C.14}$$

which is similar to our plastic yield criterion. Equation (C.14) indicates that when $\mu = 0.0$, the failure threshold is independent of pressure, p. It is a straight line at $\tau = \tau_0$, the cohesion of the material. Failure occurs when the deviatoric part of the stress matrix, $\frac{\sigma_1 - \sigma_3}{2}$, is equal to τ_0. If τ_0 in the Coulomb Failure Criterion is given the same value as τ_0 in the plastic yield criterion, and μ is set equal to zero, the two methodologies should produce similar answers. Of course, if $\mu > 0.0$, such as $\mu = 0.6$, the results for Coulomb Failure will become more complicated as shown in Figure C.3.

For our simulations of Coulomb Failure, we create random heterogeneous principal stresses, σ_1, σ_2, and σ_3, and random orientations $(\omega,[\theta,\phi])$, as described in Chapter 3. We scale the pressure, p, to the desired level, add a background stress, $\boldsymbol{\sigma}_B$, set the cohesion, τ_0, so the failure threshold will be close to Mohr circles for our points, then bring points to failure by applying a tectonic stress rate, $\dot{\boldsymbol{\sigma}}_T$. For the Coulomb Failure Criterion, failure is determined by looking at the ratio of principal stresses; hence, the failure criterion no longer uses an invariant quantity to determine failure, independent of coordinate system. The methodology involves adding an increment of stress, using the stress rate, $\dot{\boldsymbol{\sigma}}_T$, recalculating the principal stresses, checking for failure, adding another increment of stress, etc.

Figures C.2 and C.3 show the results of some of our calculations. Our heterogeneous stress in these calculations has $\alpha = 0.0$. The background stress added is $\boldsymbol{\sigma}_{B_2}$, the background stress for our "Southern San Andreas Fault" simulations from Chapter 4. We plot three different heterogeneity ratios for Figures C.2 and C.3, $HR = 0.1$, 1.0, and 10. In all the P-T axes plots for Figures C.2 and C.3, we show the first 1,000 failures using the Coulomb Fracture Criterion for a grid of 100,001 points.

On the left column in Figure C.2, we have $\mu = 0.0$ and $\textit{Pressure Ratio} = 0.0$. This should produce results similar to our plastic yield criterion, and indeed it does. The heterogeneous scatter of the P-T axes increases with increasing HR, and there is an average rotation of the P-T axes orientations with increasing HR, a rotation toward the stress rate tensor, $\dot{\boldsymbol{\sigma}}_T$. On the right column in Figure C.2, we show P-T plots for $\mu = 0.0$ and $\textit{Pressure Ratio} = 1.0$. A $\textit{Pressure Ratio} = 1.0$ means that $\dfrac{\textit{Mean}(\textit{Pressure})}{\sqrt{\textit{Mean}(\textit{Spatially Heterogeneous } I_2')}} = 1.0$. Adding this amount of pressure in our simulations has little to no effect. It may reduce the scatter of the P-T axes a small amount, but again there is still the increasing bias toward the stress rate tensor, $\dot{\boldsymbol{\sigma}}_T$, as HR increases.

The left column of Figure C.3 is the same as the right column in Figure C.2, P-T plots for $\alpha = 0.0$, $\mu = 0.0$, and $\textit{Pressure Ratio} = 1.0$. The right column changes the coefficient of friction to $\mu = 0.6$. We randomly choose between the two possible conjugate planes and plot their corresponding P-T axes. Since the conjugate planes are no longer perpendicular, there is a bifurcation of the P-T axes that is especially evident for $HR = 0.1$ in the top row. As HR increases, the scatter due to the heterogeneity

begins to connect these two separate clusters of P-T axes as seen for $HR = 1.0$ in the middle row. Then as HR increases to $HR = 10.0$, the P-T axes are so scattered it is difficult to distinguish any pattern. In general, even for $\mu = 0.6$, Coulomb Fracture, we see both of the effects observed in the plastic criterion for increasing HR: 1) Increasing scatter of the P-T axes and 2) Increasing bias toward the stress rate, $\dot{\boldsymbol{\sigma}}_T$. The two sets of P-T axes for $\mu = 0.6$ simply complicate the results; thus why we use the plastic yield criterion for the rest of the simulations in this thesis.

Coloumb Failure, α = 0.0, HR = 0.1, μ = 0.0, Pressure = 0.0

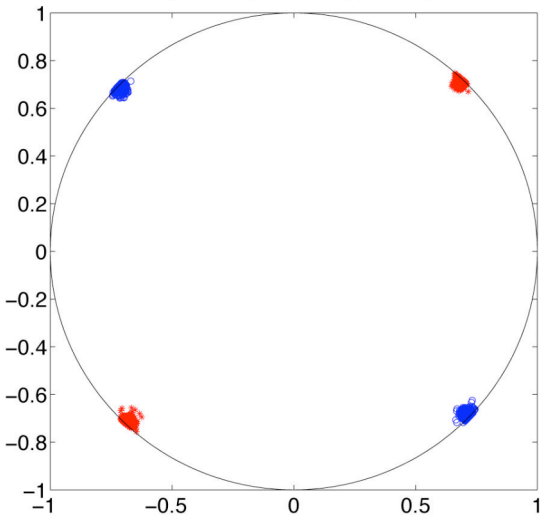

Coloumb Failure, α = 0.0, HR = 0.1, μ = 0.0, Pressure = 1.0

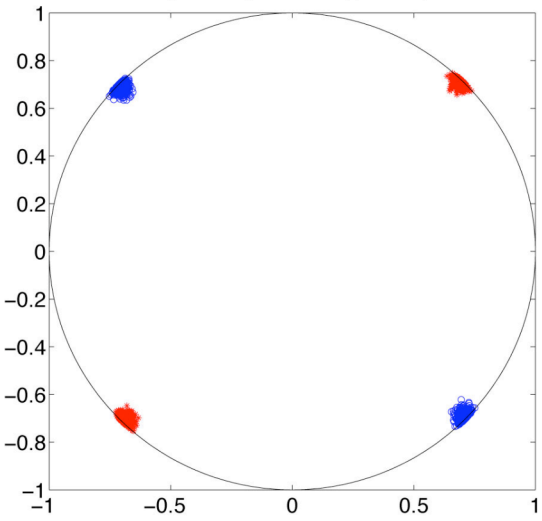

Coloumb Failure, α = 0.0, HR = 1.0, μ = 0.0, Pressure = 0.0

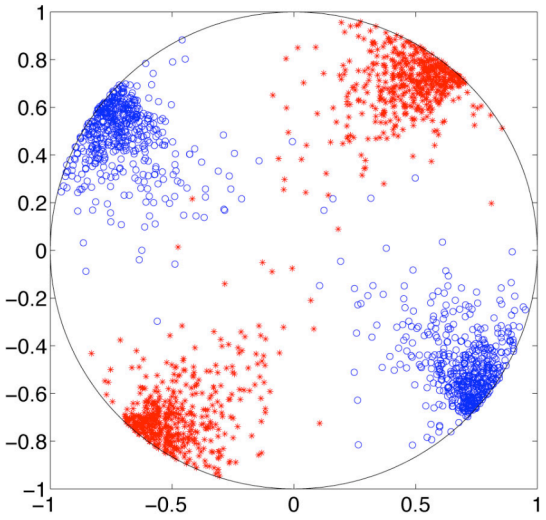

Coloumb Failure, α = 0.0, HR = 1.0, μ = 0.0, Pressure = 1.0

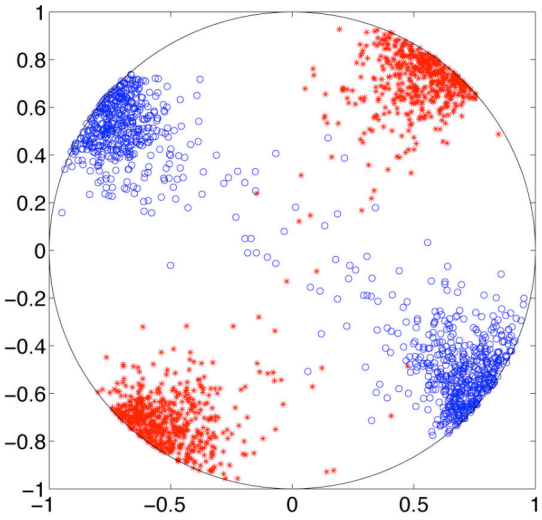

Coloumb Failure, α = 0.0, HR = 10.0, μ = 0.0, Pressure = 0.0

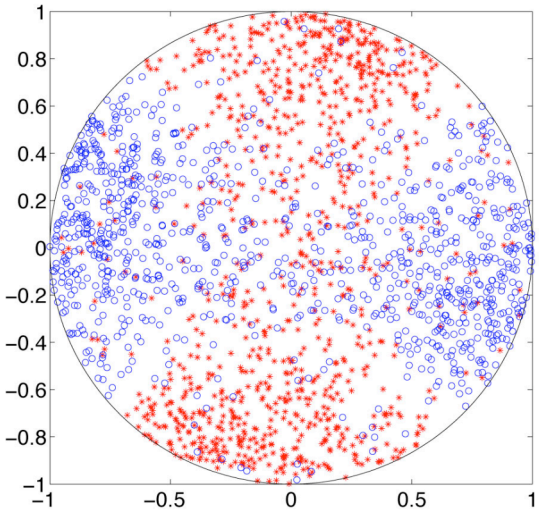

Coloumb Failure, α = 0.0, HR = 10.0, μ = 0.0, Pressure = 1.0

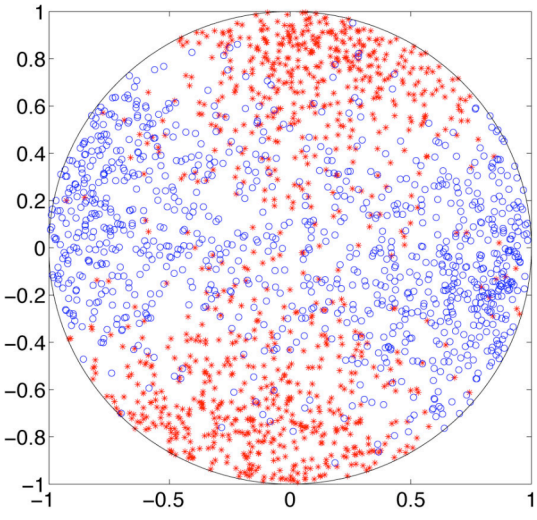

Figure C.2. *Results from our Coulomb Fracture simulations. P-T axes for the first 1,000 failures from a 100,001 point grid with* $\alpha = 0.0$ *and* $\mu = 0.0$. *On the left, no pressure has been added to the deviatoric stress in the simulations; on the right, pressure was added so that the Pressure Ratio* $= 1.0$. *The top row compares the two sets of simulations for* $HR = 0.1$, *the middle row,* $HR = 1.0$, *and the bottom row,* $HR = 10.0$. *We find that with and without pressure, the Coulomb Failure simulations replicate two features of our plastic yield simulations: 1) Increasing P-T scatter with increasing HR and 2) Increasing bias toward the stress rate tensor,* $\dot{\boldsymbol{\sigma}}_T$, *with increasing HR, where the* $\dot{\boldsymbol{\sigma}}_T$ *has N-S compression and E-W tension.*

Coloumb Failure, α = 0.0, HR = 0.1, μ = 0.0, Pressure = 1.0

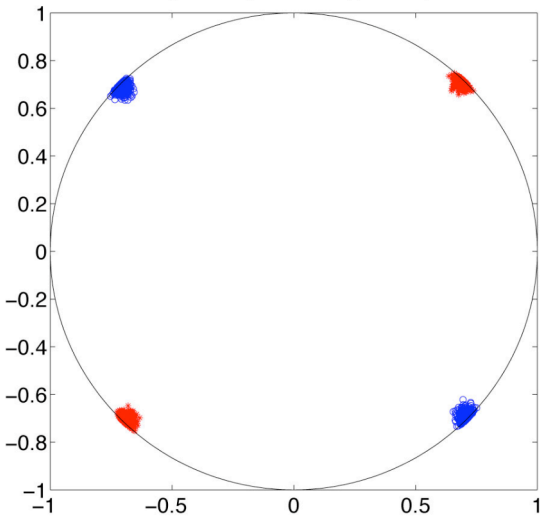

Coloumb Failure, α = 0.0, HR = 0.1, μ = 0.6, Pressure = 1.0

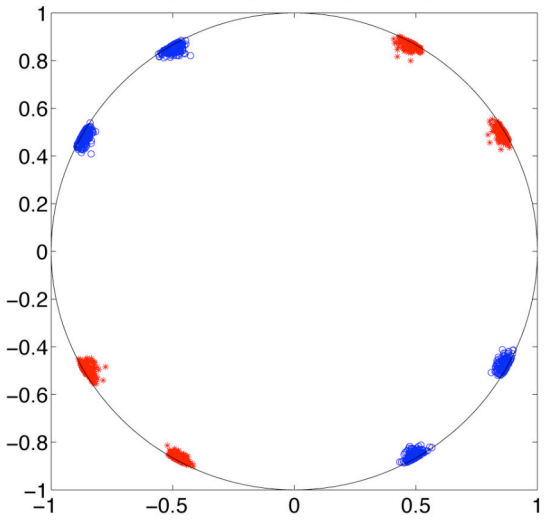

Coloumb Failure, α = 0.0, HR = 1.0, μ = 0.0, Pressure = 1.0

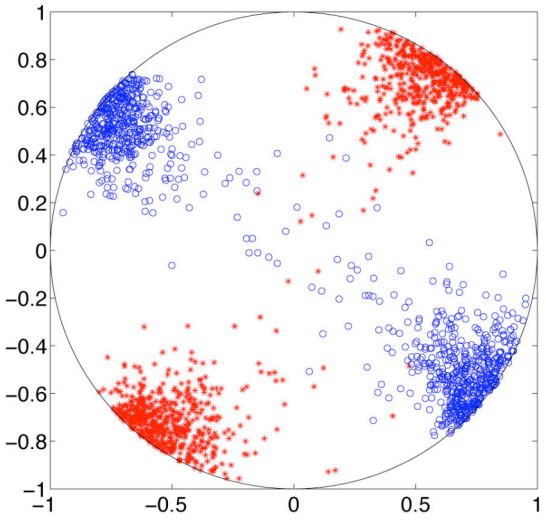

Coloumb Failure, α = 0.0, HR = 1.0, μ = 0.6, Pressure = 1.0

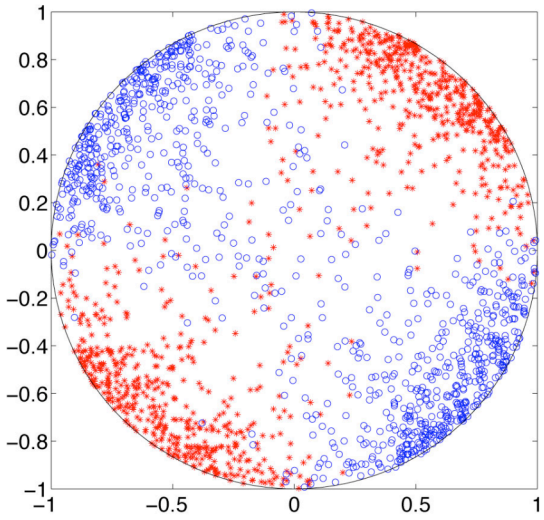

Coloumb Failure, α = 0.0, HR = 10.0, μ = 0.0, Pressure = 1.0

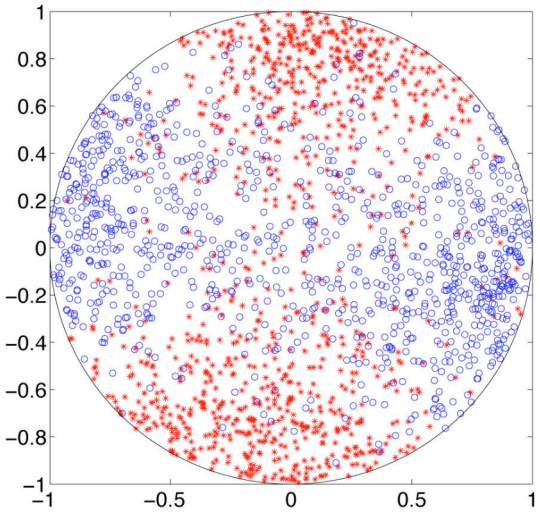

Coloumb Failure, α = 0.0, HR = 10.0, μ = 0.6, Pressure = 1.0

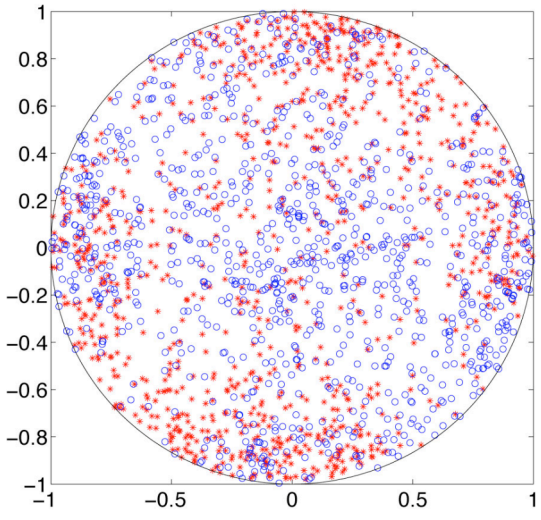

Figure C.3. *Results from our Coulomb Fracture simulations. P-T axes for the first 1,000 failures from a 100,001 point grid with* $\alpha = 0.0$ *and Pressure Ratio* $= 1.0$. *On the left,* $\mu = 0.0$, *and on the right* $\mu = 0.6$. *The left column contains the same P-T plots as the right column in Figure C.2. The top row compares the two sets of simulations for* $HR = 0.1$, *the middle row,* $HR = 1.0$, *and the bottom row,* $HR = 10.0$. *We find that regardless of the coefficient of friction,* μ, *these Coulomb Failure simulations generally replicate two features we find in our plastic yield simulations: 1) Increasing P-T scatter with increasing* HR *and 2) Increasing bias toward the stress rate tensor,* $\dot{\boldsymbol{\sigma}}_T$, *with increasing* HR, *where the* $\dot{\boldsymbol{\sigma}}_T$ *has N-S compression and E-W tension. The only problem is that for* $\mu > 0.0$ *(right column), the conjugate failure planes are no longer perpendicular; hence, if we randomly choose which failure plane we use, each cluster of P and T axes now bifurcates, greatly complicating the results. As* HR *increases to 1.0, the spatial heterogeneity of stress begins to connect two separate clusters, and as* HR *increases to 10.0, it is difficult to see a coherent pattern.*